Supporting Information:

Solving a problem with a single parameter: A smooth *bcc* to *fcc* phase transition for metallic lithium

Paul Jerabek,[*,†] Anthony Burrows,[‡] and Peter Schwerdtfeger[*,‡]

†*Institute of Hydrogen Technology, Helmholtz-Zentrum Hereon, Max-Planck-Strasse 1, D-21502 Geesthacht, Germany*

‡*Centre for Theoretical Chemistry and Physics, The New Zealand Institute for Advanced Study, Massey University Auckland, Private Bag 102904, 0745 Auckland, New Zealand*

E-mail: paul.jerabek@hereon.de; peter.schwerdtfeger@gmail.com

This electronic supplementary material contains details of the calculations using the programs VASP and Phonopy, a Table T1 with solid state properties from different density functional calculations and additional Figures F1–F7 for the thermodynamic properties.

Figures F8–F10 show the calculated densities of state for *bcc* and *fcc* Li.

Two additional separate files are also provided to the supplementary information:

1. A spreadsheet file called "FreeEnergyContributions.xlsx" detailing individual terms for the free energy including electronic and vibrational energy and entropy contributions.

2. A movie called "MartensiticTransformation.mp4" showing the movement in the cuboidal transformation along the lattice parameter A.

Contents

1 Computational Details

The lattice vector definitions in Eq. (1) of the main paper were utilized to generate primitive unit cells with $1/3 \leq A \leq 1$ (step size $\Delta A = 0.01$) along the cuboidal transformation path. The $r_{\min}$ for the primitive unit cells defined by each A value were obtained by identifying the r with the lowest energy within a range (2 Å $\leq r \leq 4$ Å) with step size $\Delta r = 0.05$ Å. Employing the periodic DFT program VASP 5.4.4,[1,2] which uses the projector augmented wave (PAW) method, single-point energies $E(r)$ were calculated. From this, $r_{\min}$ for every A value was obtained through an eighth-order polynomial fit of the $E(r)$ curve to locate the energy minimum.

Careful convergence tests regarding **k**-spacing, energy cut-off as well as different partial occupancy methods ("smearing") resulted in the following INCAR settings that were used throughout the calculations:

```
ENCUT = 1000
KSPACING = 0.075
KGAMMA = TRUE
EDIFF  = 1E-07
LREAL  = FALSE
NELMIN = 20
ISMEAR = -5
ADDGRID = TRUE
```

We tested a variety of different density functional types, LDA, GGAs (PBE, PBEsol), long-range dispersion corrected GGAs (PBE-D3, PBEsol-D3) as well as meta-GGAs (TPSS, SCAN). For the GGA functionals PBE[3] and PBEsol[4] and LDA , the POTCAR files "potPAW54_PBE/Li_sv" and "potPAW54_LDA/Li_sv" were employed, respectively, that consider the 1s semi-core states as valence states and provide in general a better description due to a higher flexibility. However, for the functionals TPSS[5] and SCAN,[6] the regular

POTCAR file "potPAW54_PBE/Li" was utilized because meta-GGAs require information about the kinetic energy density that in not included into the "Li_sv" pseudo-potential. Long-range dispersion effects were considered for the GGAs by using the D3 van-der-Waals correction together with Becke-Johnson damping.[7,8] All functionals display more or less the same general behaviour. Owing to the relatively small energy differences between the appearing structures in the range of 1 kJ/mol, rather demanding accuracy settings had to be applied (large cut-off energy for the plane-wave basis set and a very densely packed k-point grid) to ensure smooth convergence behaviour during the scans.

All functionals display more or less the same general behaviour. Owing to the relatively small energy differences between the appearing structures in the range of 1 kJ/mol, rather demanding accuracy settings had to be applied (large cut-off energy for the plane-wave basis set and a very densely packed k-point grid) to ensure a smooth convergence behaviour during the scans.

To obtain the free energy contributions (Eq. 5) for each A value, the phonon spectra for selected values ($A = 1/3$–1.0 in steps of 0.1) were computed for the PBE functional utilizing density functional perturbation theory (DFPT) and Phonopy 2.10.1.[9]

From this, $r_{\min}$ for every A value was obtained through an eighth-order polynomial fit of the $E(r)$ curve to locate the energy minimum. We note that the function $r_{\min}(A)$ exhibits a slight scattering behaviour, which we attribute to remaining numerical noise during the localization of the respective energy minima despite the demanding accuracy settings in VASP. However, the functions $E(A)$ that were calculated using the somewhat scattered $r_{\min}$ values appear very smooth, from which we deduce that the obtained $r_{\min}(A)$ functions are accurate enough for subsequent utilization and interpretation.

For the phonon calculations, $6 \times 6 \times 6$ super-cells were generated employing the previously determined $r_{\min}$ values that result in lattice constants of at least 15 Å in every direction in order to avoid self-interaction between the atoms within the periodic boundary conditions. Phonopy 2.10.0[9] was used to compute force constants of the constructed supercells necessary

for the phonon spectra calculation utilizing density functional perturbation theory (DFPT) with a Γ-centered $3 \times 3 \times 3$ k-point grid and otherwise the same INCAR settings as listed above. The (relatively small) eigenmode with negative curvature at the transition state is well localised on the atomic position and correlates well with the transition path.

The temperature-dependent thermal contributions to electronic properties ($E_{\mathrm{therm}}^{\mathrm{ele}}$ and $S_{\mathrm{therm}}^{\mathrm{ele}}$, respectively; see below) were estimated via VASP single point calculations of the supercells by setting partial occupancies according to the Fermi-Dirac distribution (ISMEAR= -1) and choosing the respective electronic temperature accordingly via the smearing width (SIGMA).

To obtain information about Li in different crystal structures (*fcc*, *bcc* and *hcp*), respective unit cells with different volumes ($\pm$ 5% around equilibrium) were generated by utilizing the scaling parameter in the POSCAR file and their energies were calculated with VASP using the same settings as before. The resulting $E(V)$ curve for each structure was fitted to the Birch-Murnaghan equation, that allowed extraction of various parameters. [10]

To obtain cohesive energies, the reference energies of a free Li atom in the centre of a slightly orthorhombic unit cell with lattice constants $14 \times 14.002 \times 14.004$ Å^3 were computed for the different functionals using the previously shown settings, only within a Γ-only k-point setting and enabling spin polarization (ISPIN = 2). The optimized lattice parameters and corresponding cohesive energies at different levels of density functional theory are shown in Table T1.

2 Calculation of Thermodynamic Properties

For the thermodynamic properties, which are dependent on the parameter A and temperature T, the following relations were used,

$$F(T, A) = E_{\mathrm{coh}}(A) + E_{\mathrm{ZPV}}(A) + E_{\mathrm{therm}}(T, A) - T S(T, A) \tag{S1}$$

where E_{ZPV} is the zero-point vibrational energy contribution, E_{therm} arises from the thermal occupation of both phonon and electron states

$$E_{\text{therm}}(T, A) = E_{\text{therm}}^{\text{vib}}(T, A) + E_{\text{therm}}^{\text{ele}}(T, A), \tag{S2}$$

and S is the vibrational and electronic contribution to the entropy

$$S(T, A) = S_{\text{therm}}^{\text{vib}}(T, A) + S_{\text{therm}}^{\text{ele}}(T, A). \tag{S3}$$

The different thermodynamic contributions are shown in Figs. F1–F7. The individual terms are defined as follows.

$$E_{\text{therm}}^{\text{vib}}(T, A) = \int_0^\infty \frac{\hbar\omega(A)e^{\frac{-\hbar\omega(A)}{k_B T}}}{(1 - e^{\frac{-\hbar\omega(A)}{k_B T}})} P(\omega, A)\mathrm{d}\omega \tag{S4}$$

where $P(\omega, A)$ describes he phonon density of states (PDOS) dependent on the lattice parameter A. The electronic term to the energy is more complicated and usually approximated by a one-particle picture through a (temperature-independent) electron density of states (EDOS or simply DOS) $D(\varepsilon, A)$ for a spin-polarized system,[11]

$$E_{\text{therm}}^{\text{ele}}(T, A) = \int_0^\infty f(\varepsilon, A, T)D(\varepsilon, A)\mathrm{d}\varepsilon \tag{S5}$$

with

$$f(\varepsilon, A, T) = \left(1 + e^{\frac{\varepsilon(A) - \varepsilon_F(A)}{k_B T}}\right)^{-1}, \tag{S6}$$

where ε_F is the Fermi energy. The term S5 was included, however, Figs. F3 and F4 below shows that this term could safely be neglected for the temperatures considered here and within the approximations used.

For the entropy we have the vibrational contribution

$$S_{\text{therm}}^{\text{vib}}(T, A) = \frac{1}{k_B T} \int_0^\infty \frac{\hbar\omega(A)}{\left(e^{\frac{\hbar\omega(A)}{k_B T}} - 1\right)} P(\omega, A)\mathrm{d}\omega - \int_0^\infty \ln[1 - e^{\frac{-\hbar\omega(A)}{k_B T}}]P(\omega, A)\mathrm{d}\omega \qquad \text{(S7)}$$

and the electronic contribution

$$S_{\text{therm}}^{\text{ele}}(T, A) = k_B \int_0^\infty s(\varepsilon, A, T)D(\varepsilon, A)\mathrm{d}\varepsilon, \qquad \text{(S8)}$$

where the function $s(\varepsilon, A, T)$ is defined by

$$s(\varepsilon, A, T) = -\{f(\varepsilon, A, T) \ln f(\varepsilon, A, T) + [1 - f(\varepsilon, A, T)] \ln[1 - f(\varepsilon, A, T)]\} \qquad \text{(S9)}$$

and again, the electronic entropy contribution is small, but not negligible as Figs. F3 and F4 below show.

Lastly, Fig. F7 shows differences in the individual contributions, i.e.

$$\Delta\mathrm{F}(T) = F(T, A = 1/2) - F(T, A = 1) \qquad \text{(S10)}$$

for the Helmholtz free energy, between *bcc* and *fcc* along the parameter A at different temperature T.

Here it is revealed that the free energy difference between *bcc* and *fcc* mainly stems from differences in entropic contributions: While the vibrational contribution to entropy clearly favours *bcc* with increasing temperature, the electronic contribution to entropy actually slightly stabilizes *fcc* with higher T values. This stabilization in the latter case can be understood from the fact that $S_{\text{therm}}^{\text{ele}}(T, A)$ $D(\varepsilon, A)$, which gives a higher entropy for the *fcc* compared to the *bcc* phase due to the number of nearest neighbour interactions.

3 Supplementary Table

Table T1: Calculated solid-state Properties for lithium at different levels of theory. Total energies E_0 in eV/atom, bulk modulus B in GPa, volume V in Å^3, cohesive energy E_{coh} (taken as positive values) in eV/atom, and nearest neighbour distance r_{min} in Å from various density functional approximations for the *bcc*, *fcc* and *hcp* lattices. The difference in cohesive energies between the *bcc* and the two *fcc/hcp* structures, $\Delta E_{\mathrm{coh}} = E_{\mathrm{coh}}(bcc) - E_{\mathrm{coh}}(fcc/hcp)$, are given in 10^{-3} eV.

|	PBE	PBE-D3	PBEsol	PBEsol-D3	LDA	TPSS	SCAN	PBE0	HSE06
E_0 (Li atom)	-0.2977	-0.2981	-0.2872	-0.2876	-0.2336	-1.0086	-0.7754	-0.6126	-0.4238
bcc	PBE	PBE-D3	PBEsol	PBEsol-D3	LDA	TPSS	SCAN	PBE0	HSE06
E_0	-1.905	-2.083	-1.9672	-2.124	-2.0449	-2.6452	-2.341	-2.1354	-1.9808
B	13.816	15.742	13.726	15.711	15.294	13.526	13.776	13.418	13.48
V_{min}	20.236	18.313	20.22	18.419	18.965	20.64	20.863	20.671	20.627
E_{coh}	-1.607	-1.785	-1.68	-1.836	-1.811	-1.637	-1.566	-1.523	-1.557
r_{min}	2.9734	2.8761	2.9726	2.8816	2.9098	2.9931	3.0038	2.9945	2.9924
fcc	PBE	PBE-D3	PBEsol	PBEsol-D3	LDA	TPSS	SCAN	PBE0	HSE06
E_0	-1.9067	-2.0852	-1.9688	-2.1261	-2.0471	-2.6467	-2.3428	-2.1426	-1.9849
B	13.942	15.659	13.748	15.482	14.98	13.611	13.999	13.441	13.463
V_{min}	20.199	18.222	20.182	18.355	18.908	20.597	20.801	20.59	20.569
E_{coh}	-1.609	-1.787	-1.682	-1.838	-1.813	-1.638	-1.567	-1.53	-1.561
ΔE_{coh}	1.6	2.2	1.6	2.1	2.2	1.4	1.8	7.2	4.1
r_{min}	3.057	2.9538	3.0562	2.961	2.9905	3.077	3.0871	3.0766	3.0756
hcp	PBE	PBE-D3	PBEsol	PBEsol-D3	LDA	TPSS	SCAN	PBE0	HSE06
E_0	-1.9065	-2.0849	-1.9687	-2.1258	-2.0468	-2.6466	-2.3429	-2.1391	-1.9832
B	13.779	15.692	13.585	15.633	30.519	13.485	13.657	26.614	26.607
V_{min}	20.209	18.254	20.192	18.384	18.927	20.609	20.802	20.573	20.599
E_{coh}	-1.609	-1.787	-1.682	-1.838	-1.813	-1.638	-1.567	-1.527	-1.559
ΔE_{coh}	1.5	1.9	1.5	1.9	1.9	1.3	1.9	3.7	2.5
r_{min}	3.0601	2.9556	3.0566	2.9626	2.9914	3.0776	3.0871	3.0758	3.0771

4 Supplementary Figures
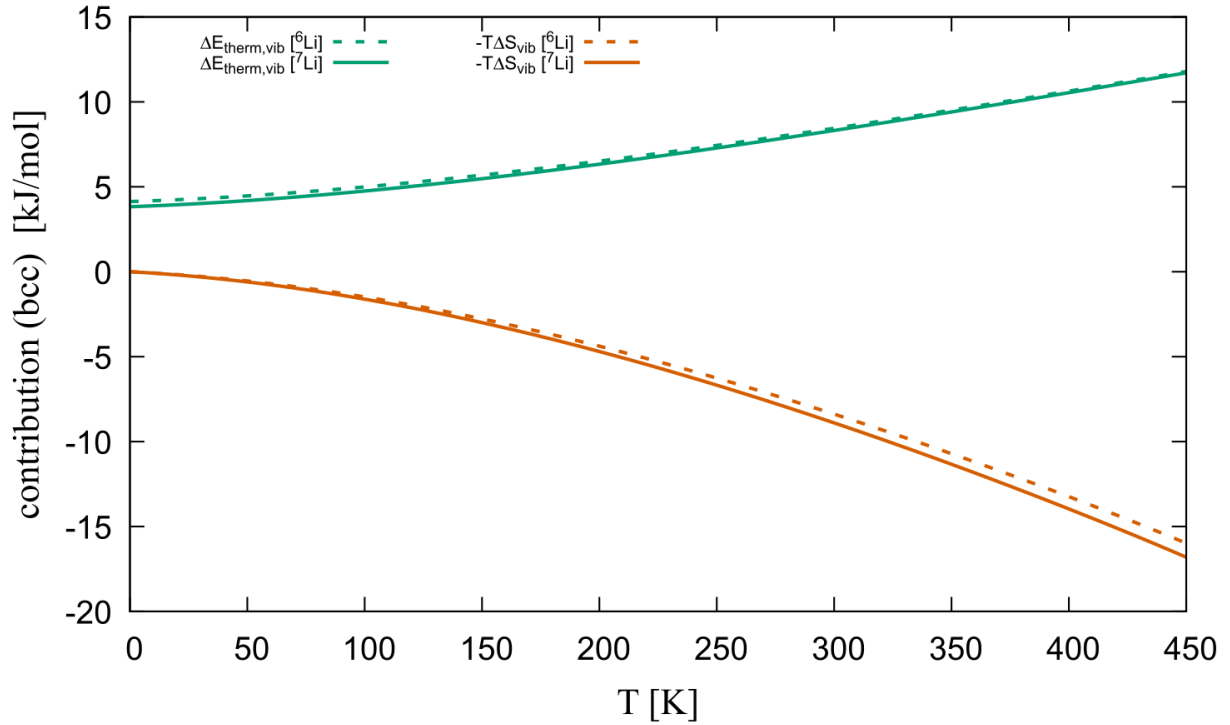
Figure F1: Calculated vibrational contribution to the free energy according to Eqs. S1 and S4, $\Delta E_{\text{therm,vib}}(T) = E_{\text{ZPV}} + E_{\text{therm}}(T)$, and Eq. S7 for the $TS_{\text{therm}}^{\text{vib}}(T)$ term, at the PBE level of theory for the *bcc* structure ($A = 1/2$) of the two ^{6}Li and ^{7}Li isotopes. The finite non-zero value at 0 K reflects E_{ZPV}.
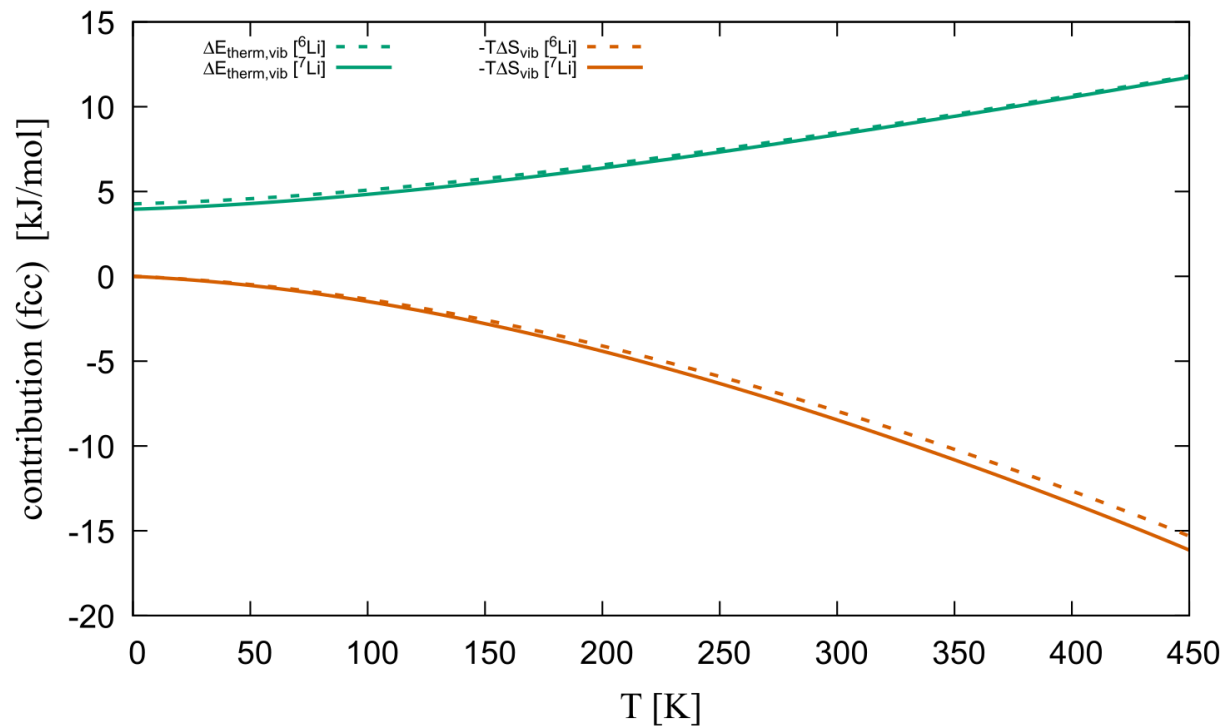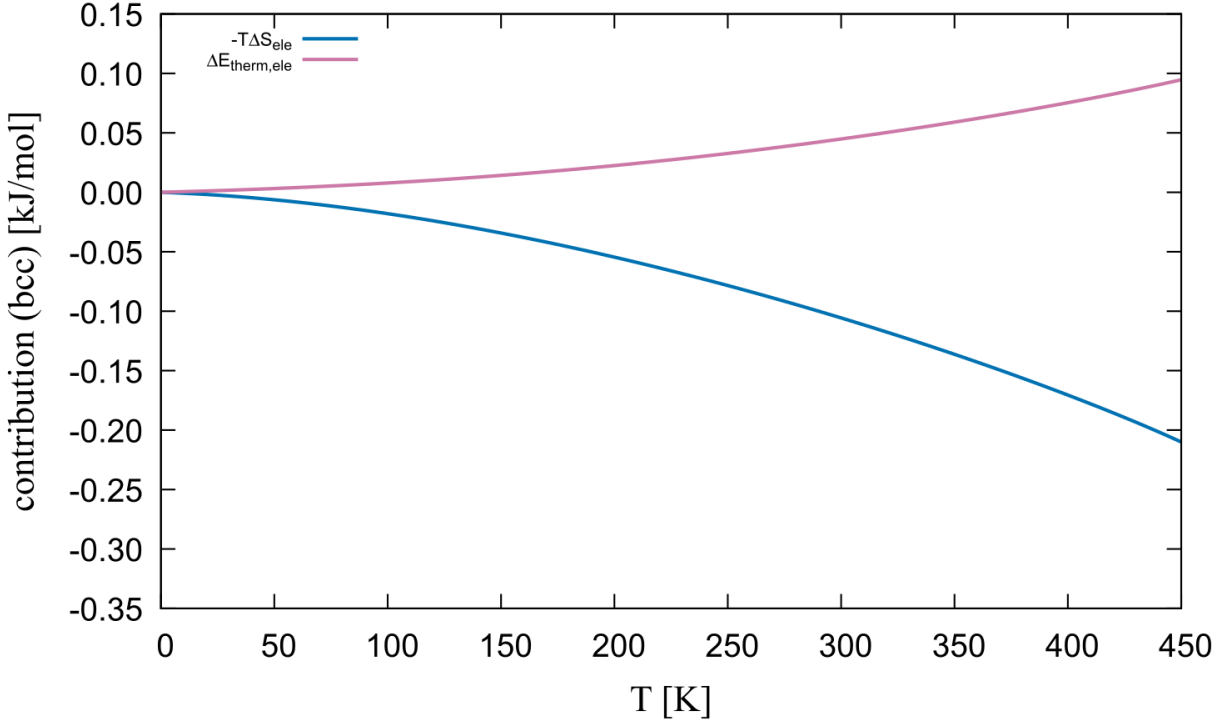
Figure F2: Calculated vibrational contribution to the free energy according to Eqs. S1 and S4, $\Delta E_{\text{therm,vib}}(T) = E_{\text{ZPV}} + E_{\text{therm}}(T)$, and Eq. S7 for the $TS_{\text{therm}}^{\text{vib}}(T)$ term, at the PBE level of theory for the *fcc* structure ($A = 1$) of the two ^{6}Li and ^{7}Li isotopes. The finite non-zero value at 0 K reflects E_{ZPV}.

Figure F3: Calculated electronic contribution to the free energy according to Eqs. S1, S5 and S8 at the PBE level of theory for the *bcc* structure ($A = 1/2$) of the two ^{6}Li and ^{7}Li isotopes.
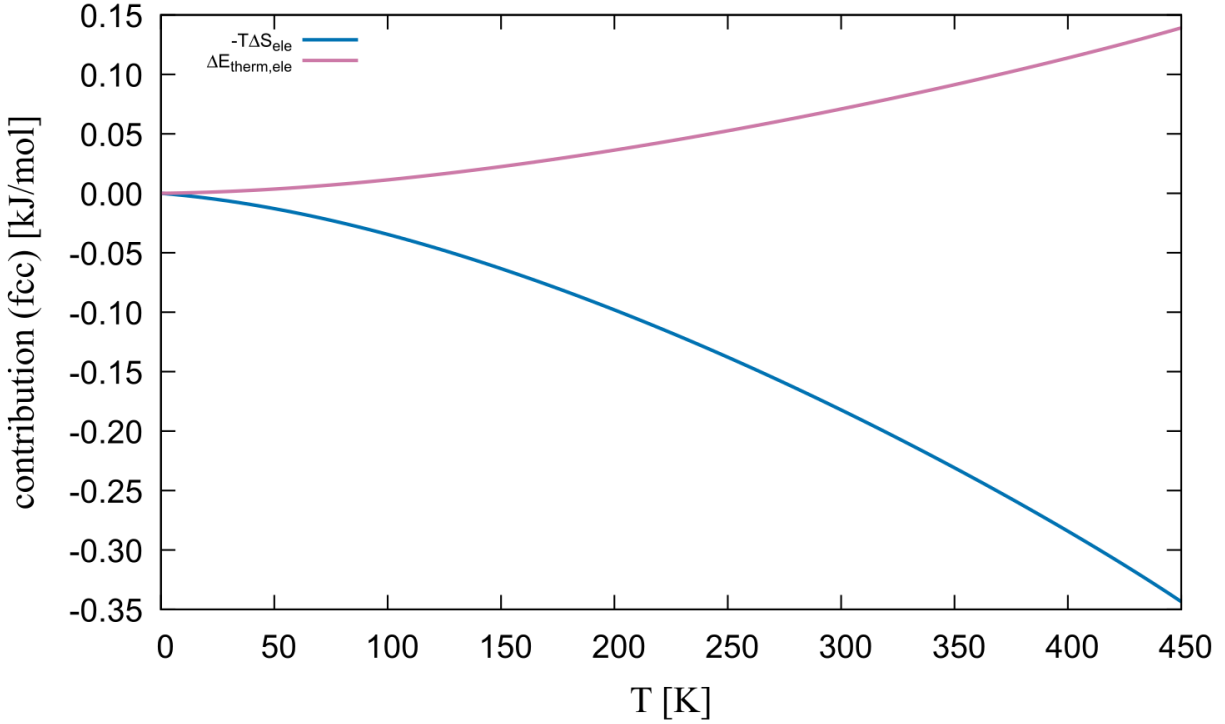
Figure F4: Calculated electronic contribution to the free energy according to Eqs. S1, S5 and S8 at the PBE level of theory for the *fcc* structure ($A = 1$) of the two ^{6}Li and ^{7}Li isotopes.
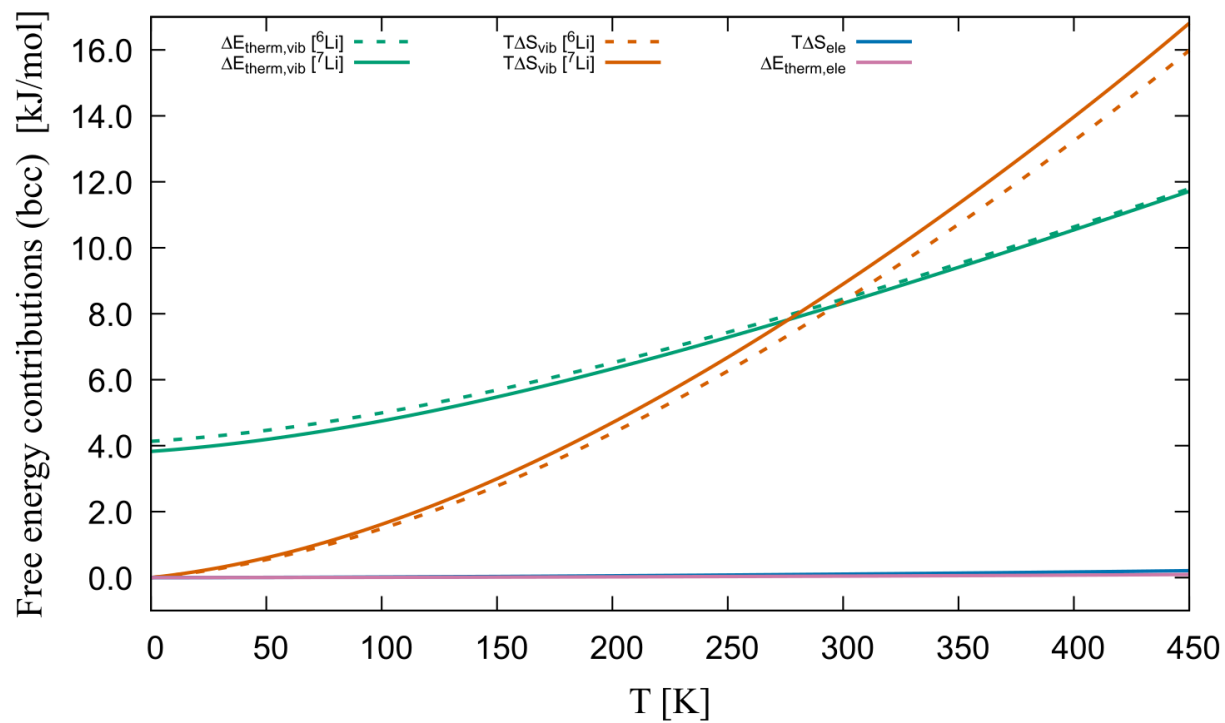
Figure F5: Calculated electronic and vibrational contributions to the free energy according to Eq. S1 (as shown in Figs. F1 and F3) for the *bcc* structure ($A = 1/2$) at the PBE level of theory for the two ^{6}Li and ^{7}Li isotopes.
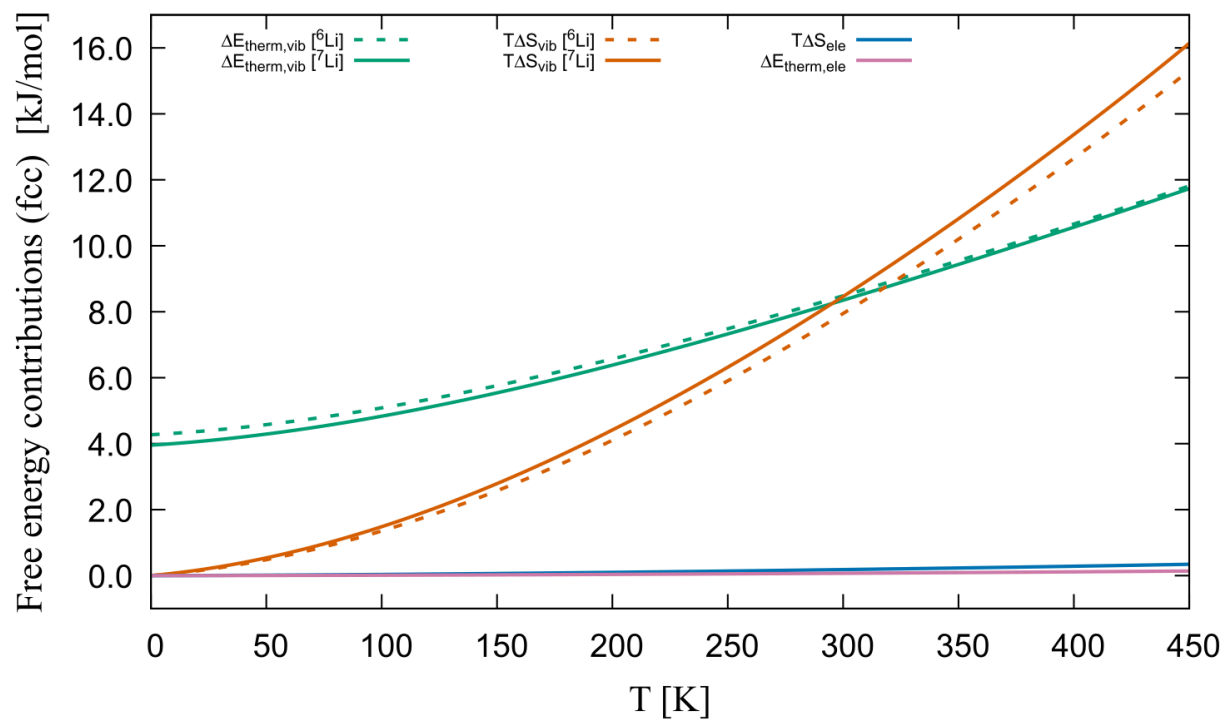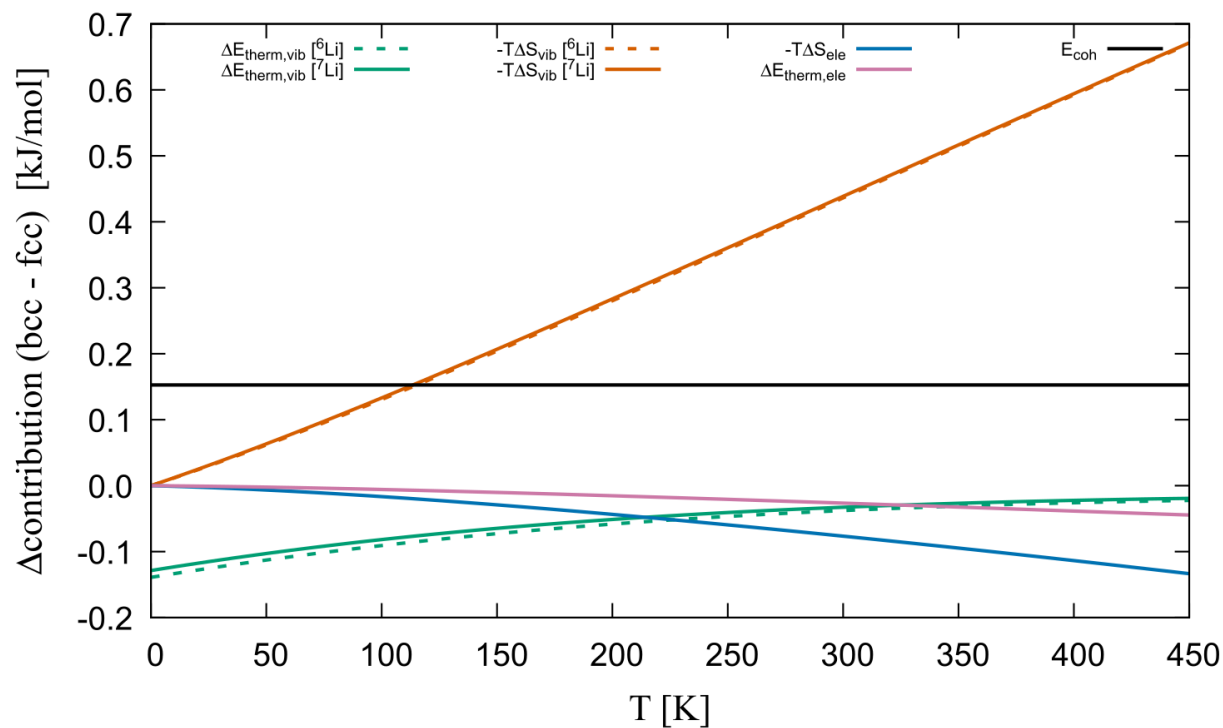
Figure F6: Calculated electronic and vibrational contributions to the free energy according to Eq. S1 (as shown in Figs. F2 and F4) for the *fcc* structure ($A = 1$) at the PBE level of theory for the two ^{6}Li and ^{7}Li isotopes.

Figure F7: Calculated differences of electronic and vibrational contributions to the free energy according to Eq. S1 (as shown in Figs. F1–F4) between the *bcc* structure ($A = 1/2$) and *fcc* ($A = 1$) structures at the PBE level of theory for the two ^{6}Li and ^{7}Li isotopes.
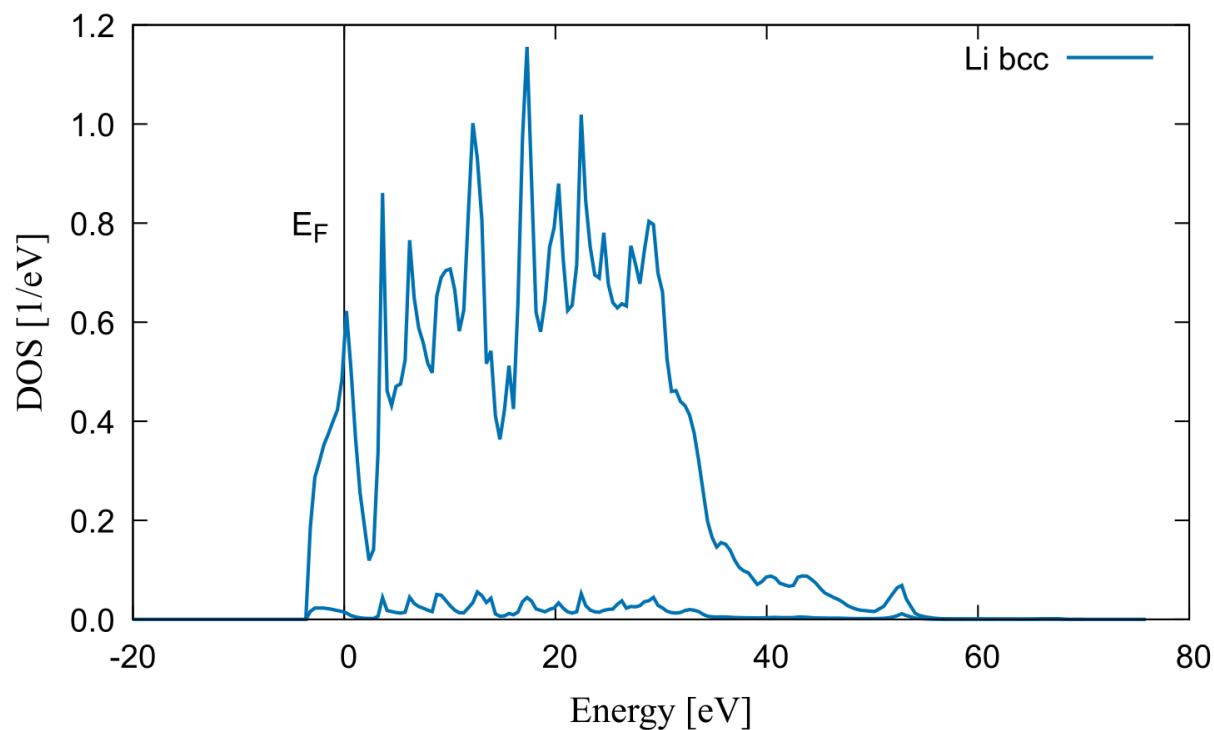
Figure F8: Calculated density of states around the Fermi level for *bcc* Li at the PBE level of theory. The zero of the energy scale was shifted to the Fermi energy (EF).
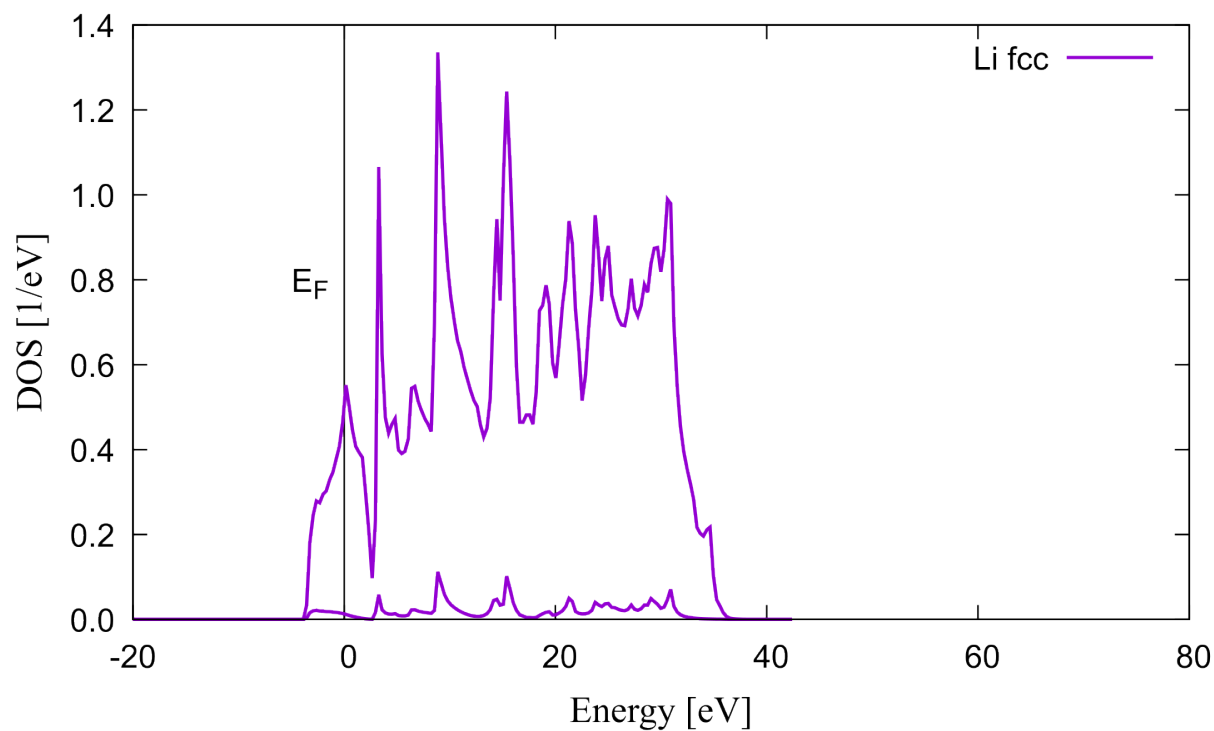

Figure F9: Calculated density of states around the Fermi level for *fcc* Li at the PBE level of theory. The zero of the energy scale was shifted to the Fermi energy (EF).
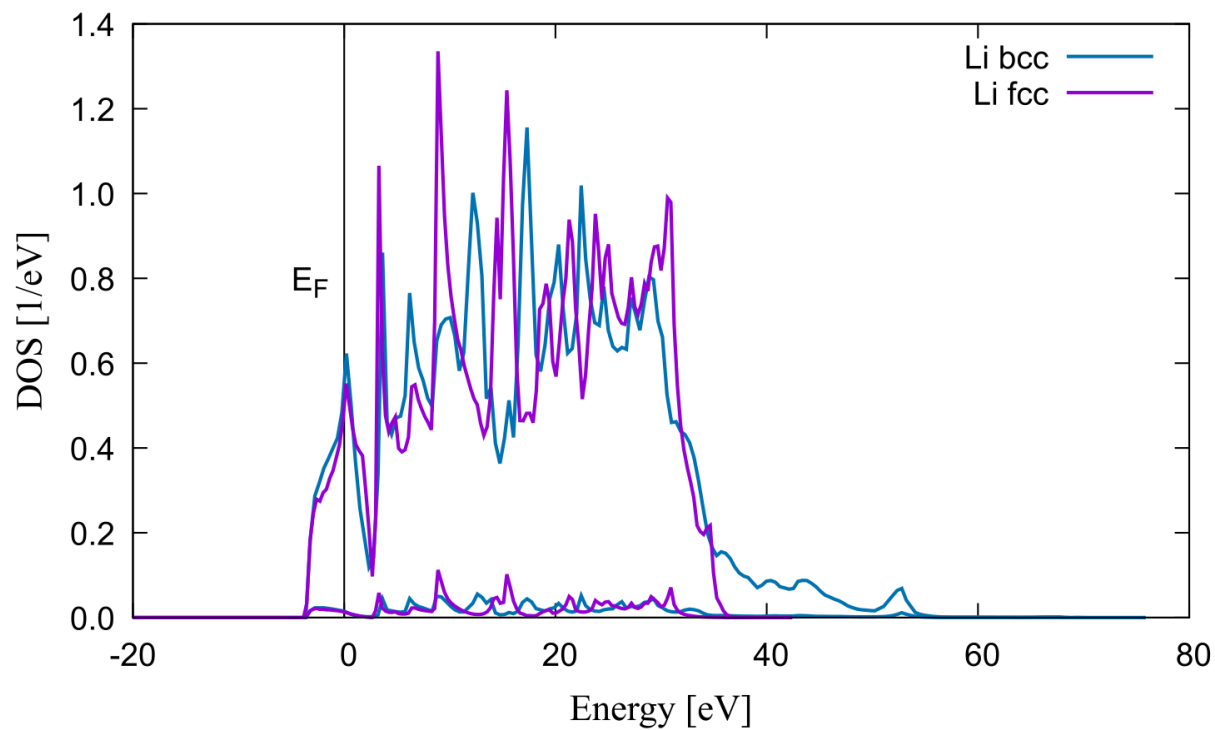
Figure F10: Calculated density of states around the Fermi level showing *bcc* and *fcc* Li in comparison at the PBE level of theory. The zero of the energy scale was shifted to the Fermi energy (EF).

References

(1) Kresse, G.; Joubert, D. *Phys. Rev. B 59*, 1758–1775.

(2) Kresse, G.; Furthmüller, J. *Phys. Rev. B 54*, 11169–11186.

(3) Perdew, J.; Burke, K.; Ernzerhof, M. *Phys. Rev. Lett 77*, 3865–3868.

(4) Csonka, G.; Perdew, J.; Ruzsinszky, A.; Philipsen, P.; Lebègue, S.; Paier, J.; Vydrov, O.; Ángyán, J. *Phys. Rev. B 79*, 155107.

(5) Sun, J.; Marsman, M.; Csonka, G.; Ruzsinszky, A.; Hao, P.; Kim, Y.-S.; Kresse, G.; Perdew, J. *Phys. Rev. B 84*, 035117.

(6) Sun, J.; Ruzsinszky, A.; Perdew, J. *Phys. Rev. Lett 115*, 036402.

(7) Grimme, S.; Antony, J.; Ehrlich, S.; Krieg, H. *J. Chem. Phys 132*, 154104–154104.

(8) Grimme, S.; Ehrlich, S.; Goerigk, L. *J. Comp. Chem 32*, 1456–1465.

(9) Togo, A.; Tanaka, I. *Scripta Materialia 108*, 1–5.

(10) Birch, F. *Phys. Rev 71*, 809–824.

(11) Zhang, X.; Grabowski, B.; Körmann, F.; Freysoldt, C.; Neugebauer, J. *Phys. Rev. B 95*, 165126.